

# Testing the Space-Time Structure of Event Generators

In memory of Klaus Kinder-Geiger

U. Heinz<sup>a,b</sup> and U.A. Wiedemann<sup>c</sup>

<sup>a</sup>*Theoretical Physics Division, CERN, CH-1211 Geneva 23*

<sup>b</sup>*Institut für Theoretische Physik, Universität Regensburg, D-93040 Regensburg*

<sup>c</sup>*Physics Department, Columbia University, New York, NY 10027*

*Combined presentation of the talks given by the two authors at the workshop  
“RHIC Physics and Beyond – Kay Kay Gee Day”  
Brookhaven National Laboratory, 23 October 1998*

**Abstract.** We report on work done in collaboration with Klaus Kinder-Geiger and John Ellis which aims at connecting the space-time structure of event generator simulations with observable output.

Klaus Geiger was an important driving force in our search for understanding the dynamics of ultrarelativistic heavy-ion collisions and quark-gluon plasma. An unconventional and unique character – this is how we will remember him. Physics was his passion, but he also loved his Porsche and his MG (=“Ma Geiger”). It is hard for us to accept that by his untimely death Klaus, whose research was dedicated so much to the future, in particular to the RHIC program at Brookhaven, should be imprisoned forever in the past. As his friends and collaborators, we will try to carry on his legacy.

## I INTRODUCTION

The main focus of Klaus’ work during the last years of his life was the event generator VNI which describes relativistic heavy-ion collisions and high energy particle collisions in terms of a perturbative parton shower Monte Carlo in phase-space combined with a simple space-time hadronization prescription. A partonic starting point is certainly required at ultrarelativistic collision energies,  $\sqrt{s} \gtrsim 100 A$  GeV, where perturbative contributions start to account for a significant part of the measured particle production. With his Parton Cascade Model [1], later amended

by a space-time hadronization algorithm [2] and made publicly available in form of the event generator VNI [3], Klaus Geiger led the way.

From summer 1997 until Klaus' death we collaborated with him and John Ellis on implementing an afterburner for Bose-Einstein correlations into this code and testing it in simulations for  $e^+e^-$  collisions at LEP I and LEP II collisions. Our goal was to prepare for an experimental test of the space-time dynamics predicted by VNI and to provide theoretical guidance for multi-dimensional Bose-Einstein analyses of various event classes with hadronic final states generated at LEP. This work [4,5] was interrupted prematurely; our contribution gives an account of the present status.

VNI distinguishes itself from many other high energy event Monte Carlos by following the event history in phase-space, not only in momentum space. *Space-time aspects* enter in the numerical simulation in various ways: On the *microscopic* level, the rescattering between produced partons or hadrons is controlled by geometric cross sections, and hadronization is modelled geometrically by requiring partons to get (in their pair rest frame) closer than 0.8 fm in coordinate space in order to form a hadronic cluster. On a *macroscopic* level this leads to a strong density dependence of particle production and absorption rates, further affected by the collective expansion of the system which is generated by the rescattering. Finally, quantum statistical effects among the produced final state particles, in particular Bose-Einstein correlations in momentum space between pairs of identical pions or kaons, depend on the *phase-space density* of the system at the point of decoupling and thus on both the momentum-space and space-time structure of the event at "freeze-out" (i.e. at the point of the last strong interaction between the particles).

In this sense all measured quantities in a heavy-ion collision depend to some extent on the space-time structure of the reaction zone. The crucial question is, however, whether they are sufficiently sensitive to such aspects to allow for a reconstruction of the space-time geometry and dynamics. The successful reproduction of single-particle yields and spectra by event generators with different space-time features, or none at all like the popular JETSET [6] and PYTHIA [7] generators, seems to argue against such a possibility. Two-particle correlations in momentum space, however, are sensitive to both the geometric extension of the "fireball" at freeze-out and to its collective expansion dynamics [8]. The latter affects the two-particle spectra via so-called " $x$ - $p$ -correlations" in the emission function  $S(x, p)$ . This function is the quantum mechanical analogue of the single-particle phase-space density of the source at freeze-out: collective expansion correlates the average direction and magnitude of the momenta of the emitted particles with their emission points. A detailed analysis of 2-pion and 2-kaon correlations in relativistic heavy-ion collisions at the Brookhaven AGS and the CERN SPS has recently led to an unambiguous demonstration of strong collective dynamics of the fireballs created in these experiments [9]. On a finer level, however, there remain a number of open physical questions whose resolution requires two-particle correlation data of similar quality and detail from elementary particle collisions. Such data do not exist, and another motivation for our work with Klaus Geiger was therefore to provide stimulation for

similar experimental analyses of high-statistics high energy data samples like the  $\sim 20$  million hadronic  $Z^0$  decays collected at LEP I.

For sufficiently high secondary particle multiplicities (i.e. at very high energies or for large collision systems) it is reasonable to assume that the two particles of a selected pair were emitted independently. This allows to express the two-particle correlation function in terms of the single-particle Wigner density  $S(x, p)$  of the source [8]. Neglecting final state interactions (assuming that they can be corrected for experimentally [8,9] or theoretically [10] at a later stage), it is given by [8]

$$C(\mathbf{q}, \mathbf{K}) = \mathcal{N} \left( 1 + \frac{|\int d^4x S(x, K) e^{iq \cdot x}|^2}{\int d^4x S(x, p_1) \int d^4y S(y, p_2)} \right). \quad (1)$$

Here  $p_1, p_2$  are the on-shell momenta of the two particles in the pair while  $K = (p_1 + p_2)/2$  and  $q = p_1 - p_2$  are their average and relative 4-momenta. The numerator in the second term stands for the product of the measured single-particle spectra

$$E_p \frac{dN}{d^3p} = \int d^4x S(x, p) \quad (2)$$

where  $p^0 = E_p = \sqrt{m^2 + \mathbf{p}^2}$ . The normalization  $\mathcal{N}$  will be discussed below.

If, for a given momentum  $K$ , the space-time dependence of  $S(x, K)$  can be characterized with reasonable accuracy by a single set of rms widths (i.e. the particle emission is not characterized by several widely differing length scales), one can approximate  $S(x, K)$  by a Gaussian in  $x$ . The correlation function then takes the simple form [8]

$$C(\mathbf{q}, \mathbf{K}) = \mathcal{N} \left( 1 + e^{-q^\mu q^\nu \langle \tilde{x}_\mu \tilde{x}_\nu \rangle (K)} \right), \quad (3)$$

where  $\langle \tilde{x}_\mu \tilde{x}_\nu \rangle (K)$  describes the second space-time moments (rms widths or ‘‘homogeneity lengths’’) of the *effective source* of particles with momentum  $K$ . Since the two measured particles are on-shell,  $p_1^2 = p_2^2 = m^2$ ,  $K \cdot q = 0$  and only 3 of the 4 components of  $q$  are independent. Different choices for the independent components lead to different Gaussian parametrizations of the correlation function [8]. We will here use the Cartesian parametrization which eliminates  $q^0 = \boldsymbol{\beta} \cdot \mathbf{q}$  where  $\boldsymbol{\beta} = \mathbf{K}/K^0$  is (approximately) the velocity of the particle pair.  $\mathbf{q}$  is decomposed into its Cartesian components  $(q_o, q_s, q_l)$  where  $l$  denotes the ‘‘longitudinal’’ direction (in heavy-ion collisions this is the direction of the beam axis, in  $e^+e^-$  collisions the direction of the thrust axis),  $o$  denotes the outward direction, fixed by the azimuthal orientation of the transverse pair momentum  $\mathbf{K}_\perp$  around the  $l$ -axis, and  $s$  denotes the third Cartesian (sideward) direction (defined by  $K_s = 0$ ,  $\mathbf{K} = (K_\perp, 0, K_l)$ ).

Eliminating  $q^0$  from the exponent in (3) leaves a sum over 6 terms; using furthermore the azimuthal symmetry of the event sample around the  $l$ -axis allows to further reduce this to 4 terms involving certain algebraic sums [8] of the rms widths

$\langle \tilde{x}_\mu \tilde{x}_\nu \rangle(K)$ . So far, however, Bose-Einstein correlations in elementary particle collisions have been parametrized by much simpler Gaussian forms, involving only one or at most two ( $K$ -independent!) size parameters. Such incomplete parametrizations have the fundamental disadvantage that the fit parameter(s) mix(es) the interesting space-time information contained in the rms widths  $\langle \tilde{x}_\mu \tilde{x}_\nu \rangle(K)$  of the effective source of particles with momentum  $K$  in such a way that they can no longer be recovered [11]. An important goal of our work with Klaus was to make predictions for the multidimensional shape of the correlation function  $C(\mathbf{q}, \mathbf{K})$ , by calculating the complete set of size parameters and their  $K$ -dependence.

The latter is particularly interesting since it signals  $x$ - $K$ -correlations in the emission function  $S(x, K)$ . While in heavy-ion collisions the dominant mechanism for such correlations appears to be collective expansion of the fireball [11,8,9], contaminations from resonance decays after freeze-out [12] and from  $x$ - $p$ -correlations in the primary hadron formation process [13] (e.g. from string fragmentation) are known to exist. The latter are expected to play a much bigger role in elementary particle collisions where a multidimensional analysis of Bose-Einstein correlations may help to isolate them. This would provide crucial input into a quantitative discussion of Bose-Einstein correlations from heavy-ion collisions where, contrary to elementary particle collisions where the multiplicities are much lower, most resonance decays can *not* be reconstructed experimentally and their effects must therefore be simulated.

## II FROM PHASE-SPACE DENSITIES TO MOMENTUM CORRELATIONS

Event generators like VNI evolve classical *probabilities*, not quantum mechanical *amplitudes* calculated from properly symmetrized many-particle wave functions. The Bose-Einstein correlations among pairs of identical pions or kaons must thus be included *a posteriori*. For notational convenience, we restrict the following discussion to a single particle species, say like-sign pions. Let us assume that we have generated  $N_{\text{ev}}$  collision events, and let the  $m$ th event ( $1 \leq m \leq N_{\text{ev}}$ ) consist of  $N_m$  such pions in the final state, emitted as free particles from the phase-space points  $\{(\tilde{\mathbf{r}}_i, \tilde{\mathbf{p}}_i, \tilde{t}_i)\}_{i \in [1, N_m]}$ . For  $N_{\text{ev}}$  events, the event generator thus simulates a classical phase-space distribution

$$\rho_{\text{class}}(\mathbf{r}, \mathbf{p}, t) = \frac{1}{N_{\text{ev}}} \sum_{m=1}^{N_{\text{ev}}} \sum_{i=1}^{N_m} \delta^{(3)}(\mathbf{r} - \tilde{\mathbf{r}}_i) \delta^{(3)}(\mathbf{p} - \tilde{\mathbf{p}}_i) \delta(t - \tilde{t}_i). \quad (4)$$

What is needed to calculate two-particle Bose-Einstein correlations according to (1) is a prescription which relates this classical phase-space density with the quantum mechanical single-particle Wigner density  $S(x, p)$  of the pion source which is supposed to be Monte Carlo simulated by the event generator. In sections IIB and IIA, we focus on two different interpretations of the event generator output

which we call “classical” and “quantum”, respectively, although these names should not distract from the fact that conceptually both are on an equal footing. Each one of them leads to a different algorithm for calculating the two-particle correlation function from the event generator output:

$$\left\{ \{(\check{\mathbf{r}}_i, \check{\mathbf{p}}_i, \check{t}_i)\}_{i \in [1, N_m]}\right\}_{m \in [1, N_{\text{ev}}]} \implies C(\mathbf{q}, \mathbf{K}), \quad (5)$$

Before discussing them we list three requirements which any such algorithm should fulfill:

1. Since the event generator evolves classical probabilities, not symmetrized production amplitudes, the generated momenta  $\check{\mathbf{p}}_i, \check{\mathbf{p}}_j$  do not show the enhanced probability at low relative momenta  $\check{\mathbf{p}}_i - \check{\mathbf{p}}_j$  characteristic for Bose-Einstein final state symmetrization. The prescriptions (5) should calculate this effect a posteriori.
2. The strength of Bose-Einstein correlations depends on the distance of the identical particles in phase-space, not in momentum space. We thus require the prescriptions (5) to use the entire phase-space information, and not only the generated momentum information. ‘Weighting’ or ‘shifting’ prescriptions which are based only on the latter [6] may successfully match the measured momentum correlations but obviously do not allow to test the simulated space-time structure.
3. In general, Bose-Einstein statistics can affect particle multiplicity distributions during the particle production process but classical event generators do not include such effects explicitly. Nevertheless they are tuned to reproduce the measured average particle multiplicities  $\langle N \rangle$ . In order not to destroy this tuning we require that the prescription (5) conserves the single-particle multiplicities. If the event generator were also tuned to reproduce the average multiplicity of identical particle *pairs*,  $\langle N(N-1)/2 \rangle$ , i.e. to reproduce not only the mean, but also the width of the multiplicity distribution, then the prescription (5) should not change that either. Interpreting the correlator as a factor which relates the measured two-particle differential cross section to the one simulated by the event generator,  $d\sigma_{\text{meas}}/d^3p_1 d^3p_2 = C(\mathbf{q}, \mathbf{K}) d\sigma_{\text{sim}}/d^3p_1 d^3p_2$ , this then implies [4,6,14] that  $\mathcal{N} < 1$  in (1). The algorithms discussed below do not satisfy this last requirement, i.e. in general they change the width of the multiplicity distribution. However, since the space-time analysis of correlation data can be based entirely on the momentum dependence of  $C(\mathbf{q}, \mathbf{K})$ , irrespective of its absolute normalization, this does not matter for our purposes.

## A “Classical” interpretation of event generator output

In the “classical” interpretation [16,5], the phase-space points  $(\check{\mathbf{r}}_i, \check{\mathbf{p}}_i, \check{t}_i)$  are seen as a discrete approximation of the on-shell Wigner phase-space density  $S(x, p)$ :

$$S(x, \mathbf{p}) = \rho_{\text{class}}(\mathbf{x}, \mathbf{p}, t). \quad (6)$$

This defines both the two-particle correlator via (1) and the one-particle spectrum via (2). For a numerical implementation one must replace the momentum-space  $\delta$ -functions in (4) by normalized “bin functions” with finite width  $\epsilon$  of rectangular [16] or Gaussian [5] shape, e.g.

$$\delta_{\check{\mathbf{p}}, \mathbf{p}}^{(\epsilon)} = \frac{1}{(\pi\epsilon^2)^{3/2}} \exp\left(-(\check{\mathbf{p}}_i - \mathbf{p})^2/\epsilon^2\right), \quad (7)$$

which reduce to the original  $\delta$ -function in the limit  $\epsilon \rightarrow 0$ . The one-particle spectrum and two-particle correlator then read [16,5]

$$E_p \frac{dN}{d^3p} = \int d^4x S(x, \mathbf{p}) = \frac{E_p}{N_{\text{ev}}} \sum_{m=1}^{N_{\text{ev}}} \sum_{i=1}^{N_m} \delta_{\check{\mathbf{p}}, \mathbf{p}}^{(\epsilon)}, \quad (8)$$

$$C(\mathbf{q}, \mathbf{K}) = 1 + \frac{\sum_{m=1}^{N_{\text{ev}}} \left[ \left| \sum_{i=1}^{N_m} \delta_{\check{\mathbf{p}}, \mathbf{K}}^{(\epsilon)} e^{i(q^0 \check{t}_i - \mathbf{q} \cdot \check{\mathbf{r}}_i)} \right|^2 - \sum_{i=1}^{N_m} \left( \delta_{\check{\mathbf{p}}, \mathbf{K}}^{(\epsilon)} \right)^2 \right]}{\sum_{m=1}^{N_{\text{ev}}} \left[ \left( \sum_{i=1}^{N_m} \delta_{\check{\mathbf{p}}, \mathbf{p}_1}^{(\epsilon)} \right) \left( \sum_{j=1}^{N_m} \delta_{\check{\mathbf{p}}, \mathbf{p}_2}^{(\epsilon)} \right) - \sum_{i=1}^{N_m} \delta_{\check{\mathbf{p}}, \mathbf{p}_1}^{(\epsilon)} \delta_{\check{\mathbf{p}}, \mathbf{p}_2}^{(\epsilon)} \right]}. \quad (9)$$

The correlator (9) is the discretized version of the Fourier integral in (1). The subtracted terms in the numerator and denominator remove discretization errors which would amount to pairs constructed from the same particles. This “classical” algorithm, as well as the “quantum” version discussed below, is numerically efficient since it involves only  $O(N_m)$  manipulations per event. The calculated observables, while being discrete functions of the input, are continuous functions of the measured momenta, i.e. no binning in  $\mathbf{q}, \mathbf{K}$  is necessary.

## B “Quantum” interpretation of event generator output

The “quantum” interpretation [16,15,14,5] of the event generator output starts from the observation that, for a given event, i.e. a single term in the sum of (4), the simultaneous sharp definition of the particle momenta and positions at emission violates the uncertainty relation. In the limit  $N_{\text{ev}} \rightarrow \infty$  the sum is still expected to be a smooth phase-space function and, to the extent that the event generator provides an accurate simulation of the underlying QCD quantum dynamics, it is also expected to respect the uncertainty constraints on any allowed Wigner density. Since in practice, however, one has to work with finite numbers of events, one may wish to ensure consistency with the uncertainty principle on the single-event level.

This is achieved [15–17] by associating the centers of single-particle wave packets with the set of generated phase-space points  $\{ \{ (\check{\mathbf{r}}_i, \check{\mathbf{p}}_i, \check{t}_i) \}_{i \in [1, N_m]} \}_{m \in [1, N_{\text{ev}}]}$ :

$$(\check{\mathbf{p}}_i, \check{\mathbf{r}}_i, \check{t}_i) \longrightarrow f_i(\mathbf{x}, \check{t}_i) = \frac{1}{(\pi\sigma^2)^{3/4}} e^{-\frac{1}{2\sigma^2} (\mathbf{x} - \check{\mathbf{r}}_i)^2 + i\check{\mathbf{p}}_i \cdot \mathbf{x}}. \quad (10)$$

The  $f_i$  describe quantum mechanically best-localized states, i.e. they saturate the Heisenberg uncertainty relation with  $\Delta x_i = \sigma/\sqrt{2}$  and  $\Delta p_i = 1/\sqrt{2}\sigma$ .

Taking only two-particle symmetrized contributions into account (“pair approximation” [14]), all spectra can be written [16,15] in terms of the single-particle spectrum  $s_i(\mathbf{p})$  corresponding to an individual wave packet at phase-space point  $i$ :

$$E_p \frac{dN}{d^3p} = \frac{E_p}{N_{\text{ev}}} \sum_{m=1}^{N_{\text{ev}}} \nu_m(\mathbf{p}) = \frac{E_p}{N_{\text{ev}}} \sum_{m=1}^{N_{\text{ev}}} \sum_{i=1}^{N_m} s_i(\mathbf{p}), \quad (11)$$

$$C(\mathbf{q}, \mathbf{K}) = 1 + e^{-\frac{1}{2}\sigma^2 \mathbf{q}^2} \frac{\sum_{m=1}^{N_{\text{ev}}} \left[ \left| \sum_{i=1}^{N_m} s_i(\mathbf{K}) e^{i(q^0 \check{t}_i - \mathbf{q} \cdot \check{\mathbf{r}}_i)} \right|^2 - \sum_{i=1}^{N_m} s_i^2(\mathbf{K}) \right]}{\sum_{m=1}^{N_{\text{ev}}} \left[ \nu_m(\mathbf{p}_1) \nu_m(\mathbf{p}_2) - \sum_{i=1}^{N_m} s_i(\mathbf{p}_1) s_i(\mathbf{p}_2) \right]}, \quad (12)$$

$$s_i(\mathbf{p}) = \left( \frac{\sigma^2}{\pi} \right)^{3/2} e^{-\sigma^2 (\mathbf{p} - \check{\mathbf{p}}_i)^2}. \quad (13)$$

Again, the subtracted terms in the numerator and denominator of  $C(\mathbf{q}, \mathbf{K})$  are finite multiplicity corrections which become negligible for large particle multiplicities [15]. This algorithm is consistent with an emission function  $S(x, \mathbf{K})$  which is obtained by folding the classical distribution  $\rho_{\text{class}}$  of wave packet centers with the Wigner density  $s_0(x, \mathbf{K})$  of a single wave packet:

$$S(x, \mathbf{K}) = \int d^3 \check{\mathbf{r}}_i d^3 \check{\mathbf{p}}_i d\check{t}_i \rho_{\text{class}}(\check{\mathbf{r}}_i, \check{\mathbf{p}}_i, \check{t}_i) s_0(\mathbf{x} - \check{\mathbf{r}}_i, t - \check{t}_i, \mathbf{K} - \check{\mathbf{p}}_i), \quad (14)$$

$$s_0(x, \mathbf{K}) = \frac{1}{\pi^3} \delta(t) e^{-\frac{1}{\sigma^2} x^2 - \sigma^2 \mathbf{K}^2}. \quad (15)$$

The latter saturates the uncertainty relation with a spatial uncertainty  $\sigma$  and a momentum uncertainty  $1/\sigma$ , and the folding ensures that now  $S(x, \mathbf{K})$  is always quantum mechanically consistent. However, in this algorithm both the one- and two-particle spectra depend on the wave packet width  $\sigma$ . The role of this parameter will be discussed in the context of our toy model study in section III.

The “classical” and “quantum” algorithms differ only with respect to two points:

1. The “classical” algorithm has no analogue for the Gaussian prefactor  $\exp(-\frac{1}{2}\sigma^2 \mathbf{q}^2/)$  in (12) which is a genuine quantum effect stemming from the quantum mechanical localization properties of (10).
2. The Gaussian single-particle distributions  $s_i(\mathbf{p})$  in the “quantum” algorithm are the quantum analogues of the “bin functions” in the “classical” algorithm. With the Gaussian bin functions (7) the two agree for the choice  $\sigma = 1/\epsilon$ . Finite event statistics puts a lower practical limit on  $\epsilon$  in the “classical” algorithm, but to get accurate spectra one should try to choose  $\epsilon$  as small as possible, by simulating sufficiently many events. In contrast,  $\sigma$  in the “quantum” algorithm is the finite spatial width of the single-particle wave packets, and the limit  $\sigma \rightarrow \infty$  (which corresponds to  $\epsilon \rightarrow 0$ ) is not physically relevant: according to (14) it amounts to an emission function with infinite spatial extension and thus to a correlator [15]  $\lim_{\sigma \rightarrow \infty} C(\mathbf{q}, \mathbf{K}) = 1 + \delta_{\mathbf{q}, \mathbf{0}}$ .

### III THE ZAJC MODEL

Before describing realistic event generator simulations we discuss some analytical results for a classical toy model distribution  $\rho_{\text{class}}$ . These are then used to test the algorithms of sections II B and II A, by applying those to sets of phase-space points  $\{(\check{\mathbf{r}}_i, \check{\mathbf{p}}_i, \check{t}_i)\}_{i \in [1, N_m]}$  generated from the model distribution with a Monte Carlo procedure. In this way we can make quantitative statements about i) the  $\sigma$ -dependence of the “quantum” algorithm, ii) the  $\epsilon$ -dependence of the “classical” algorithm (especially: how small  $\epsilon$  has to be chosen to extract the limit  $\epsilon \rightarrow 0$  numerically) and iii) the statistical requirements for the algorithms to work.

The toy model, first introduced by Zajc [18], reads:

$$\rho_{\text{class}}^{\text{Zajc}}(\mathbf{r}, \mathbf{p}, t) = \mathcal{N}_s \delta(t) \exp \left\{ -\frac{1}{2(1-s^2)} \left( \frac{\mathbf{r}^2}{R_0^2} - 2s \frac{\mathbf{r} \cdot \mathbf{p}}{R_0 P_0} + \frac{\mathbf{p}^2}{P_0^2} \right) \right\}, \quad (16)$$

$$\mathcal{N}_s = E_p \frac{N}{(2\pi R_s P_0)^3}, \quad R_s = R_0 \sqrt{1-s^2}. \quad (17)$$

The distribution is normalized to a total event multiplicity  $N$ . The parameter  $s$  smoothly interpolates between completely position-momentum correlated and uncorrelated sources. For  $s \rightarrow 0$ , the position-momentum correlation vanishes and we are left with the product of two Gaussians in  $\mathbf{r}$  and  $\mathbf{p}$ . In the limit  $s \rightarrow 1$

$$\lim_{s \rightarrow 1} \rho_{\text{class}}^{\text{Zajc}}(\mathbf{r}, \mathbf{p}, t) \sim \delta^{(3)} \left( \frac{\mathbf{r}}{R_0} - \frac{\mathbf{p}}{P_0} \right) \delta(t), \quad (18)$$

the position-momentum correlation is perfect. The total phase-space volume of the distribution  $V_{\text{p.s.}} = (2R_s P_0)^3$  vanishes for  $s \rightarrow 1$ . This strong  $s$ -dependence allows to study the performance of our numerical algorithms for different phase space volumes. In the following subsections, we discuss the  $s$ -dependence of the one-particle spectrum and two-particle correlator, focussing in sections III A and III B on analytical results, and comparing these in section III C to numerical calculations.

#### A The Zajc model in the “classical” algorithm

Inserting (16) into (6)-(9) one finds [5]

$$E_p \frac{dN}{d^3p} = E_p \frac{N}{(2\pi P_0^2)^{3/2}} \exp \left( -\frac{\mathbf{p}^2}{2P_0^2} \right), \quad (19)$$

$$C(\mathbf{q}, \mathbf{K}) = 1 + \exp \left( -\mathbf{q}^2 R_{\text{class}}^2(\epsilon) \right), \quad (20)$$

$$R_{\text{class}}^2(\epsilon) = \frac{R_s^2}{1 + \epsilon^2/(2P_0^2)} \left( 1 + \frac{\epsilon^2}{2P_0^2(1-s^2)} - \frac{1}{(2R_s P_0)^2} \right). \quad (21)$$

We recover the physical HBT radius  $R_{\text{class}}^2 = R_s^2(1 - 1/(2R_s P_0)^2)$  from (21) in the limit  $\epsilon \rightarrow 0$  or by inserting (6) directly into (1). The remarkable fact is that for sufficiently large  $s$  [18],

$$s > s_{\text{crit}} = \sqrt{1 - \frac{1}{(2R_0P_0)^2}}, \quad (22)$$

the HBT radius  $R_{\text{class}}^2$  becomes negative and the two-particle correlator shows an unphysical rise of the correlation function with increasing  $\mathbf{q}^2$ . The change of sign in (20) seems to be related to the violation of the uncertainty relation by the emission function for large  $s$  when  $\mathbf{r}$  and  $\mathbf{p}$  become strongly correlated. At the critical value  $s_{\text{crit}}$  the phase-space volume  $V_{\text{p.s.}}$  of the source drops below 1. Only for  $s < s_{\text{crit}}$  the distribution  $\rho_{\text{class}}^{\text{Zajc}}$  is a quantum mechanically allowed emission function, i.e. a Wigner density.

The practical importance of the Zajc model in the unphysical limit  $s \geq s_{\text{crit}}$  is that it provides an extreme testing ground for our numerical algorithms. Analytically, we conclude already from (21) that in order to be close to the physical limit the bin width  $\epsilon$  has to be small on the scale of the width of the generated momentum distribution,

$$\epsilon \ll \sqrt{2} P_0. \quad (23)$$

In the above toy model this requirement is independent of the strength of position-momentum correlations in the source.

## B The Zajc model in the “quantum” algorithm

Inserting the model distribution  $\rho_{\text{class}}^{\text{Zajc}}$  into (14) (instead of (6)), we find

$$E_p \frac{dN}{d^3p} = E_p \frac{N}{(2\pi P^2)^{3/2}} \exp\left(-\frac{\mathbf{p}^2}{2P^2}\right), \quad (24)$$

$$C(\mathbf{q}, \mathbf{K}) = 1 + \exp\left(-\mathbf{q}^2 R_{\text{qm}}^2\right), \quad (25)$$

$$R_{\text{qm}}^2 = R^2 \left(1 - \frac{1}{(2RP)^2}\right), \quad (26)$$

$$R^2 = R_2^2 + \frac{\sigma^2}{2}, \quad P^2 = P_0^2 + \frac{1}{2\sigma^2}. \quad (27)$$

In this case,  $R$  and  $P$  satisfy  $2RP \geq 1$  independent of the value of  $\sigma$  and, in contrast to the “classical” algorithm, the radius parameter  $R_{\text{qm}}^2$  is now always positive, irrespective of the value of  $s$ . Even if the classical distribution  $\rho_{\text{class}}^{\text{Zajc}}(\check{\mathbf{r}}, \check{\mathbf{p}}, \check{t})$  is sharply localized in phase-space, its folding with minimum uncertainty wave packets leads to a quantum mechanically allowed emission function  $S(x, \mathbf{p})$  and to a correlator with falls off with increasing  $\mathbf{q}^2$  as expected. However, the spread of the one-particle momentum spectrum (24) receives an additional contribution  $1/\sigma^2$ . Choosing  $\sigma$  too small increases this term beyond the phenomenologically reasonable values, choosing it too large widens the corresponding HBT radius parameters significantly. It was argued [15] that  $\sigma$  can be interpreted as quantum mechanical “size” of the

particle,  $\sigma \approx 1$  fm. Given the heuristic nature of these arguments and the significant modifications this implies for the spectra (24) and (25), it is however fair to say that presently  $\sigma$  mainly plays the role of a regulator of unwanted violations of the quantum mechanical uncertainty principle while a deeper understanding of its origin in the particle production dynamics is still missing.

## C Numerical simulations in the Zajc model

We have studied the performance of our Bose-Einstein algorithms by generating with a random number generator sets  $\{(\check{\mathbf{r}}_i, \check{\mathbf{p}}_i, \check{t}_i)\}_{i \in [1, N_m]}$  of phase-space points according to the distribution  $\rho_{\text{class}}^{\text{Zajc}}$  and comparing the numerical results of our algorithms to the analytical expressions of section III A and III B.

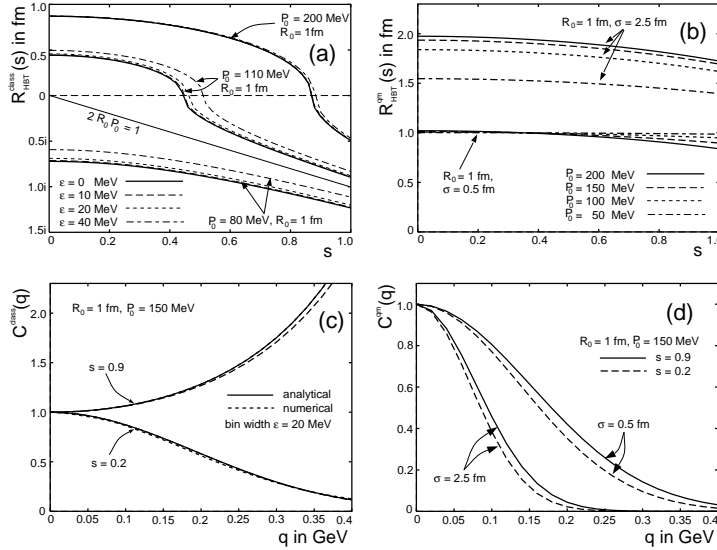


**FIGURE 1.** Generic properties of the one-dimensional Zajc model. (a): HBT-radius parameter (21) of the “classical” interpretation as a function of the position-momentum correlation  $s$ . The plot shows the HBT radius for different combinations of the model parameters  $R_0$  and  $P_0$ , and for different sizes of the bin width  $\epsilon$  used in the numerical implementation. (b): Same as (a) for the “quantum” version (26) of the model. The dependence of the HBT radius on the wave packet width  $\sigma$  is clearly seen. (c) and (d): The two-particle correlator in the “classical” (c) and “quantum” (d) version of the model for different sets of model parameters. The numerical results are obtained for 50 events of multiplicity 1000, and agree very well with the analytical calculations.

Fig. 1(a) shows the  $\epsilon$ -dependence of the HBT radius parameter (21). For fixed bin width  $\epsilon$ , the approximation of the true HBT radius parameter by  $R_{\text{class}}^2(\epsilon)$  is seen to become better with increasing  $P_0$ , in agreement with (23). For the HBT radius obtained from the “quantum” version of the Zajc model and depicted in Fig. 1(b), the situation is both qualitatively and quantitatively different. Now, the HBT radius is always positive, since the Gaussian wave packets take quantum mechanical

localization properties automatically into account. Also, the  $s$ -dependence of the radius is seen to be much weaker since the wave packets smear out the unphysically strong position-momentum correlations present in the classical distribution  $\rho_{\text{class}}^{\text{Zajc}}$ . The HBT radius depends not only on the geometrical size  $R_0$ , and on the momentum width  $P_0$  of the source, but also on the wave packet width  $\sigma$ . As seen in Fig. 1(b), this wave packet width affects the HBT radius and its  $P_0$ -dependence significantly for  $\sigma > R_0$ .

In Figs. 1(c,d) we present the two-particle correlation functions corresponding to these HBT radius parameters for characteristic values of the model parameters. The analytical results, obtained by plotting (20) and (25), are compared to the results from the event generator algorithms (12) and (9). The plot was obtained using 50 events of multiplicity 1000. The differences between analytical and numerical results originate from statistical fluctuations and become smaller with increasing number of events  $N_{\text{ev}}$  or event multiplicity  $N_m$ . The good agreement between analytical and numerical results in Figs. 1(c,d) indicates the relatively low statistical requirements of our algorithms. The reason is that both algorithms associate with the *discrete* set of generated momenta  $\check{\mathbf{p}}_i$  *continuous* functions of the measured momenta  $\mathbf{p}_1, \mathbf{p}_2$ . This smoothens any statistical fluctuation significantly. For the “classical” algorithm, small deviations between numerical and analytical results are still visible in Fig. 1(c), while the results of the “quantum” algorithm coincide within line width. This can be traced back to the Gaussian prefactor  $\exp(-\sigma^2 \mathbf{q}^2/2)$  in (12) which provides an additional smoothening of statistical fluctuations not present in the “classical” algorithm.

## IV TWO-PARTICLE CORRELATIONS FROM VNI

We have applied the “quantum” algorithm discussed above to simulated  $e^+e^-$  collisions at LEP I [19] and LEP II [20] energies from VNI. We have focussed on the channels (see Fig. 2)

$$e^+e^- \rightarrow Z^0 \rightarrow q\bar{q} \rightarrow \text{hadrons} \quad \text{at } \sqrt{s} = 91.5 \text{ GeV}, \quad (28)$$

$$e^+e^- \rightarrow W^+W^- \rightarrow q\bar{q}'q'\bar{q} \rightarrow \text{hadrons} \quad \text{at } \sqrt{s} = 183 \text{ GeV}, \quad (29)$$

which provide the “cleanest” environment for the study of Bose-Einstein correlations in high-energy particle collisions. Especially for the first channel there exists an impressively extensive and accurate data sample of several million events. For high-energy  $e^+e^-$  collisions, theoretical studies of Bose-Einstein enhancements have mainly been performed within the context of the string models [21], which have been quite successful in reproducing the distributions of identical particle pairs on the level of 1-parameter Gaussian fits of the correlator [22]. Our study [5] is based on the event generator VNI and aimed at a full inclusion of the space-time structure of the events and a multidimensional correlation analysis.

The “classical” and “quantum” interpretation of the event generator output discussed in section II A and II B provide *two different prescriptions* for the calcula-

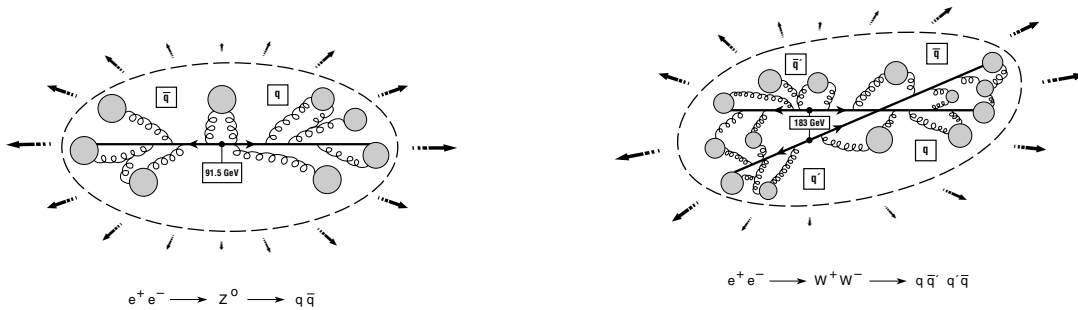


**FIGURE 2.** Schematics of the two  $e^+e^-$  event types (28) and (29): The final-state hadron distribution in  $Z^0$  events (left) is due to exclusively ‘endogamous’ hadronization of the partonic offspring from the  $q\bar{q}$  dijet, whereas in  $W^+W^-$  events (right) there is, in addition, the possibility of ‘exogamous’ hadron production involving a mating of partons from the two different  $W^+ \rightarrow q\bar{q}'$  and  $W^- \rightarrow q'\bar{q}$  dijets.

tion of two-particle correlations. This ambiguity in the calculational scheme can be traced back to the fact that both algorithms are *a posteriori* remedies for an incomplete quantum mechanical time evolution which does not account properly for the quantum mechanical symmetrization of identical  $N$ -particle states. The ambiguity has to be removed by a physical consistency requirement. From our discussion of the Zajc model in section III, first crude statements about such consistency requirements can be made:

1. The “quantum” interpretation introduces a wave packet width  $\sigma$  which must be adjusted to data. The measured HBT radius parameters provide an upper bound on  $\sigma$ ,  $\sigma < R_{\text{HBT}}$ . Hence, the “quantum” interpretation can only be consistent with experimental data if the wave packet width is not too large.
2. In order for the “classical” interpretation of the event generator output to be consistent with experimental data, the generated output must not be peaked too strongly in phase-space. Otherwise, the HBT radius may be unphysically small or even show the wrong sign, cf. section III A.

The first step in a realistic study of two-particle correlations is necessarily to refine these crude statements. To what extent do physical observables depend on the choice of algorithm? Which choice of  $\sigma$  is consistent with experiment? Are there phenomenological reasons to prefer one of the algorithms? These workshop proceedings reflect the state of our work when Klaus left us. At the time of the airline accident we had only completed the calculation with the “quantum” algorithm, and only for a single value of the wave packet width  $\sigma$ . A comparison of the two algorithms remains to be done.

## A Two-particle correlations at vanishing pair momentum

Fig. 3 shows the correlator  $C(\mathbf{q}, \mathbf{K}) - 1$  for different  $\mathbf{q}$ -values and vanishing pair momentum  $\mathbf{K}$  in the c.m. frame of the collision,  $C(q_z, q_s, q_o, \mathbf{0}) - 1$ . The widths of the correlator in three Cartesian directions are roughly the same. Quantitatively, they are roughly given by the inverse of the wave packet width  $\sigma$  which suggests that they are dominated by the “quantum mechanical smearing” features of the

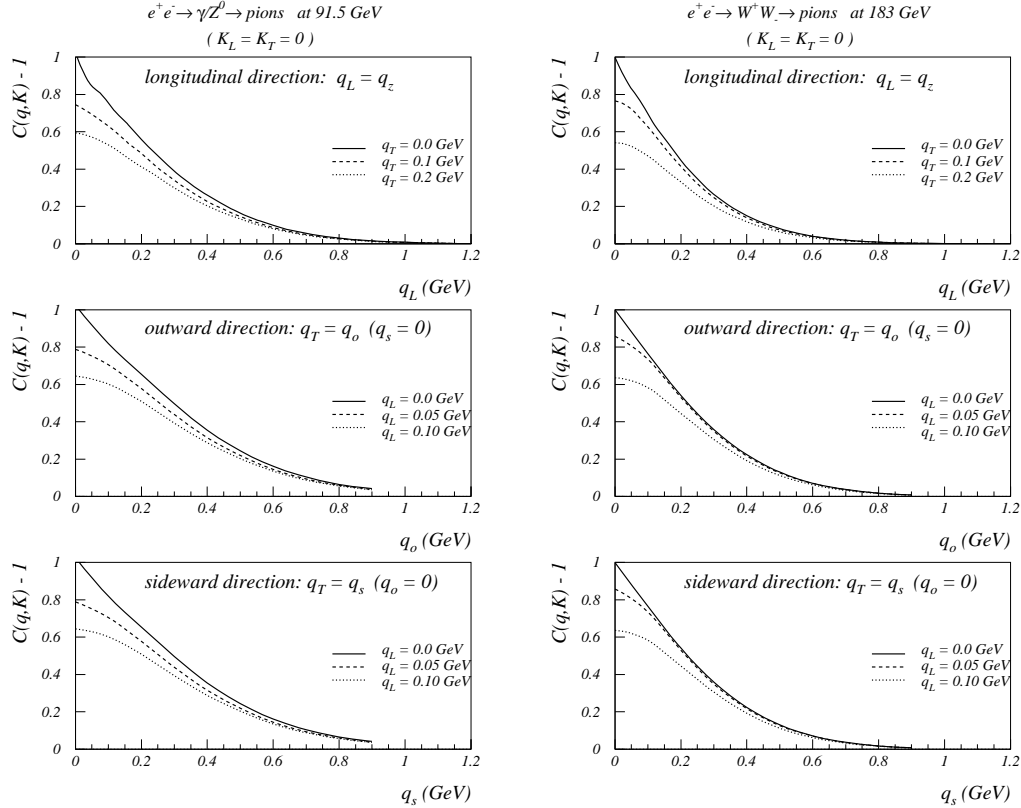


**FIGURE 3.** The correlation function of same-sign pions for different values of the relative pair momentum  $\mathbf{q}$  for vanishing pair momentum  $\mathbf{K}$ ,  $C(q_z, q_s, q_o, \mathbf{0}) - 1$ .

“quantum” Bose-Einstein algorithm used here. A simulation with the “classical” algorithm remains to be done.

One also sees that near  $\mathbf{q} = 0$  the correlation functions show characteristic deviations from a Gaussian shape. However, at non-zero values of the orthogonal  $\mathbf{q}$ -components, the correlators become nicely Gaussian. The non-Gaussian features at small  $\mathbf{q}$  can be traced to decay contributions from long-lived resonances: Fig. 4 shows the same correlator with and without such contributions. Neglecting the pions from long-lived resonance decays, the correlation function becomes Gaussian and wider, reflecting a smaller source size. With long-lived resonances included, the effective pion source  $S(x, \mathbf{K})$  is larger, resulting in a narrower and non-Gaussian correlation function. This clearly demonstrates the sensitivity of the correlation

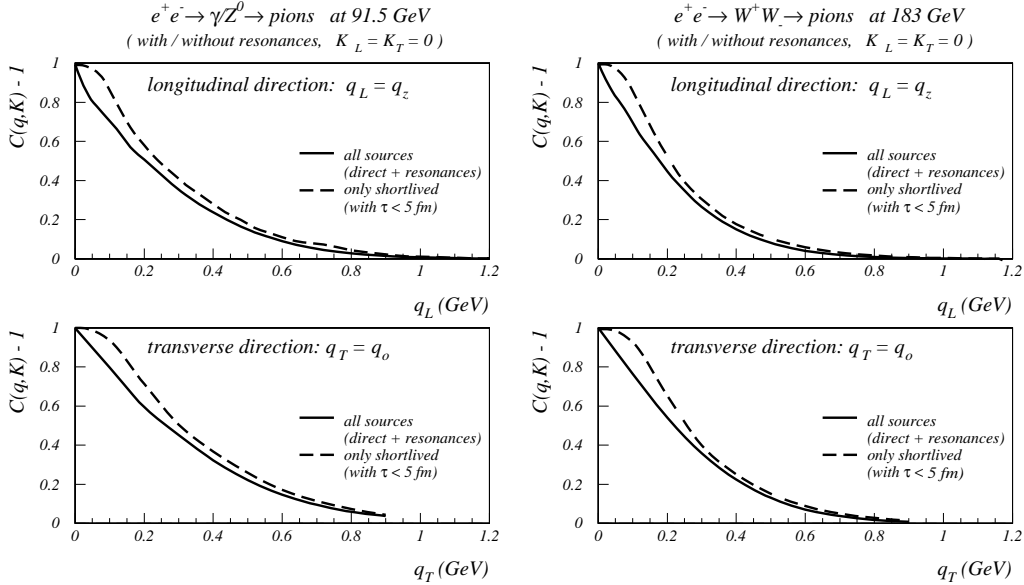


**FIGURE 4.** The correlator  $C(\mathbf{q}, \mathbf{K}) - 1$  for  $\mathbf{K} = 0$  with (solid lines) and without (dashed lines) the contributions of pions stemming from long-lived resonances.

function on the space-time *geometry* of the source function  $S(x, \mathbf{K})$ .

## B Pair momentum dependence of the correlation function

As discussed before, the dependence of the correlation function on the pair momentum  $\mathbf{K}$  indicates  $x$ - $K$ -correlations in the source and can thus be sensitive to the space-time *dynamics* of hadron production. Fig. 5 shows the correlation function  $C(\mathbf{q}, \mathbf{K}) - 1$  of same-sign pions for various values of the pair momentum  $\mathbf{K} = (K_L, \mathbf{K}_\perp)$ . Clearly, as  $\mathbf{K}$  increases, the correlation function becomes wider, indicating a smaller effective source, qualitatively (although not quantitatively) very similar to the corresponding observations in heavy-ion collisions. This is an interesting prediction which to our knowledge has not yet been tested in the LEP experiments. According to the more detailed analysis presented in [5] the observed  $\mathbf{K}$ -dependence can be fully attributed to the  $\mathbf{K}$ -dependence of resonance decay contributions; however, this may be to some extent an artifact of the employed “quantum” Bose-Einstein algorithm whose wave packet width  $\sigma$  apparently dominates the widths of the correlation functions shown above.

## V OUTLOOK

The rather abrupt ending of the above section on physics results gives a sad feeling for the gap left by Klaus. In our collaboration, he was the only one who actually knew how to run VNI. Our original motivation came from relativistic

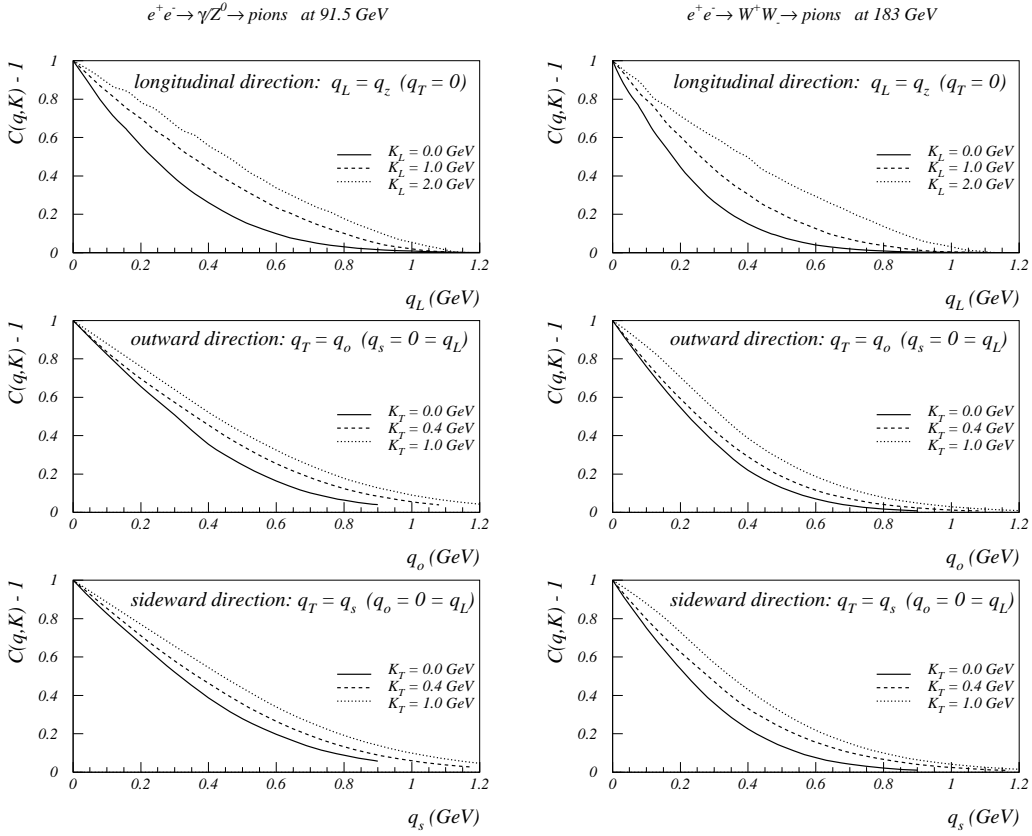


**FIGURE 5.** The correlation function of same-sign pions  $C(\mathbf{q}, \mathbf{K}) - 1$  for various values of the pair momentum  $\mathbf{K} = (K_L, \mathbf{K}_\perp)$ , where  $K_L = K_z$  is the direction along the thrust axis and  $K_\perp = |\mathbf{K}_\perp| = \sqrt{K_x^2 + K_y^2}$  is the momentum transverse to it. The correlators are plotted against one component of the relative momentum, setting the two other components to zero.

heavy-ion collisions where the space-time geometry and dynamics of the event plays a crucial role in understanding basic measurable quantities. Mainly for this reason we developed algorithms which allow to calculate identical two-particle correlation functions from an arbitrary event generator output. We tested the accuracy and statistical requirements of these algorithms in simple toy model studies and applied them in a first realistic study to the hadronic channels in  $e^+ e^-$  annihilation at the  $Z^0$ -peak and near the  $W^+W^-$  threshold. However, a comparative study of both algorithms is still missing and our main goal, the application of these algorithms to the study of event simulations of heavy ion collisions, is not achieved yet. We plan to do so in the near future. Also, we plan to make the algorithms described in section II publicly available, using the Open Standard for Codes and Routines (OSCAR) format, advocated in [23].

## REFERENCES

1. Geiger, K., and Müller, B., *Nucl. Phys. B* **369**, 600 (1992); Geiger, K., *Phys. Rev. D* **47**, 133 (1993); *Phys. Rep.* **258**, 237 (1995).
2. Ellis, J., and Geiger, K., *Nucl. Phys. A* **590**, 609c (1995); and *Phys. Rev. D* **52**, 1500 (1995).
3. Geiger, K., *Comput. Phys. Commun.* **104**, 70 (1997).
4. Wiedemann, U.A., Ellis, J., Heinz, U., and Geiger, K., in *CRIS'98: Measuring the size of things in the Universe: HBT interferometry and heavy ion physics*, (S. Costa et al., eds.), World Scientific, Singapore, 1999.
5. Geiger, K., Ellis, J., Heinz, U., and Wiedemann, U.A., hep-ph/9811270, submitted to *Phys. Rev. D*.
6. Lönnblad, L., and Sjöstrand, T., *Phys. Lett. B* **351**, 293 (1995); *Eur. Phys. J. C* **2**, 165 (1998).
7. Sjöstrand, T., *Comput. Phys. Commun.* **39**, 347 (1986); Sjöstrand, T., and Bengtsson, M., *Comput. Phys. Commun.* **43**, 367 (1987).
8. Wiedemann, U.A., and Heinz, U., nucl-th/9901094, *Phys. Rep.*, in press.
9. Heinz, U., Jacak, B.V., nucl-th/9902020, *Ann. Rev. Nucl. Part. Sci.* **49** (1999), in press.
10. Anchishkin, D.V., Heinz, U., and Renk, P., *Phys. Rev. C* **57**, 1428 (1998); Sinyukov, Yu., et al., *Phys. Lett. B* **432**, 248 (1998).
11. Heinz, U., in *Correlations and Clustering Phenomena in Subatomic Physics* (M.N. Harakeh, O. Scholten, and J.H. Koch, eds.), NATO ASI Series B **359**, 137 (1996) (Plenum, New York).
12. Schlei, B.R., Ornik, U., Plümer, M., and Weiner, R.M., *Phys. Lett. B* **293**, 275 (1992); Bolz, J., et al., *Phys. Lett. B* **300**, 404 (1993); and *Phys. Rev. D* **47**, 3860 (1993); Wiedemann, U.A., and Heinz, U., *Phys. Rev. C* **56**, R610 and 3265 (1997).
13. Bialas, A., Zalewski, K., *Acta Phys. Pol. B* **30**, 359 (1999).
14. Wiedemann, U.A., *Phys. Rev. C* **57**, 3324 (1998).
15. Wiedemann, U.A. et al., *Phys. Rev. C* **56**, R614 (1997).
16. Zhang, Q.H., Wiedemann, U.A., Slotta, C., and Heinz, U., *Phys. Lett. B* **407**, 33 (1997).
17. Merlitz, H., and Pelte, D., *Z. Phys. A* **357**, 175 (1997).
18. Zajc, W.A., in *Particle Production in Highly Excited Matter* (H.H. Gutbrod and J. Rafelski, eds.), NATO ASI Series B **303**, 435 (1993) (Plenum, New York).
19. Hebbeker, T., *Phys. Rep.* **217**, 69 (1992); Bethke, S., and Pilcher, J.E., *Ann. Rev. Nucl. Part. Sci.* **42**, 251 (1992).
20. Ballestrero, A., et al., *J. Phys. G* **24**, 365 (1998).
21. Andersson, B., Gustafson, G., Ingelman, G., and Sjöstrand, T., *Phys. Rep.* **97**, 33 (1983); Andersson, B., Gustafson, G., and Söderberg, B., *Nucl. Phys. B* **264**, 29 (1986).
22. Bowler, M.G., *Z. Phys. C* **29**, 617 (1985); Andersson, B., and Hoffmann, W., *Phys. Lett. B* **169**, 364 (1986); Andersson, B., and Ringner, M., *Phys. Lett. B* **421**, 283 (1998); Häkkinen, J., and Ringner, M., *Eur. Phys. J. C* **5**, 275 (1998).
23. Pang, Y., *Nucl. Phys. A* **638**, 219c (1998).